Performance of reverse osmosis membrane with large feed pressure fluctuations from a wave-driven desalination system

Kurban A. Sitterley[1,2,*], Tani J. Cath[1], Dale S. Jenne[2], Yi-Hsiang Yu[3], Tzahi Y. Cath[1,**]

[1]*Colorado School of Mines, Golden, CO, USA*

[2]*National Renewable Energy Laboratory, Golden, CO, USA*

[3]*National Yang Ming Chiao Tung University, Hsinchu City, Taiwan*

[*]Corresponding author, email: tcath@mines.edu, phone: +1 (720) 722-3343

[*]Co-corresponding author, email: Kurban.Sitterley@nrel.gov, phone: +1 (704) 402-4664

Submitted for possible publication in

Desalination

Submitted: August 2021

Revised: December 2021

Abstract

Wave-driven desalination systems are proposed water treatment systems that involve reverse osmosis of seawater powered directly by wave motion. Such a configuration would result in drastic feed pressure fluctuations. For a technology conventionally operated with a constant feed condition, the effect of these variable pressures on membrane integrity and performance is unknown. Experiments were conducted with spiral wound membranes coupled to a system capable of producing feed pressure fluctuations of more than 400 psi. Feed composition included 5, 20, and 35 g/L NaCl, and a synthetic seawater at normal and 1.5× concentration. The variable feed conditions included sine-like pressure waves swings of 200–500 and 500–900 psi with frequencies of 1.25, 7.5, and 12 waves/min, and a model-generated random waveform. Between each wave experiment we performed membrane integrity tests at 650 psi and 25 g/L NaCl feed, which showed a 7.4% drop in the membrane's water permeability coefficient, an 18.4% flux decline, and more than 99% salt rejection over 1,770 hours of cumulative experimental time. Analysis of permeate samples showed high salt rejection. In general, variable feed pressure had no significant deleterious effect on membrane integrity or performance.

Keywords: desalination, reverse osmosis, hydrokinetic energy, wave energy, sustainability

Highlights

- Impact of large feed pressure variations on membrane integrity were investigated
- Permeability showed no substantial decline over 1800 hours of dynamic feed pressure
- Permeate water quality did not deviate from expectations under dynamic operation

1. Introduction

The production of drinking water relies on a consistent energy source to perform the necessary treatment. Many places lack one or both resources, driving technological innovation to further enable access to safe drinking water. In coastal areas, desalination can play a role in expanding access to fresh water. Membrane desalination uses semi-permeable membranes, such as reverse osmosis (RO) or nanofiltration (NF) membranes, and high hydraulic pressure to separate salt and other contaminants from seawater and brackish water. Often, desalination is too energy intensive to implement in developing coastal communities where reliable energy is scarce; desalination technology can require up to 10 times more energy to treat per cubic meter than surface water [1]. Thus, there has been much effort into implementing desalination using sustainable and renewable energy sources and doing so can reduce associated airborne emissions by 85% and lower costs for the end user [1, 2]. There have been demonstrations and modeling of systems that use renewable (but intermittent) sources of energy, including wind [3-5], solar [6], and geothermal [2].

An often-overlooked source of renewable energy in coastal communities is energy harvested from the motion of ocean waves, or hydrokinetic energy. Waves contain an estimated 8,000–80,000 TWh/year of energy—a huge resource [1]—and many devices exist that can convert wave motion to usable energy, termed wave energy converters (WECs). Large population centers located on coastlines, including 14 of the 17 largest cities in the world, have significant potential hydrokinetic energy resources; the use of hydrokinetic energy for seawater desalination is a natural next step in the transition toward sustainable development of water resources [7]. Typically, wave energy is converted to electricity, which is then used to power desalination systems operating at a constant feed pressure [8]. Several RO systems have been designed and built that use hydrokinetic energy in different forms [9-11]. Such systems, broadly called wave-driven desalination systems (WDDS), commonly include a wave-activated body (e.g., a buoy or flapping device) that drives a fluid (air or water) through a turbine to produce electricity, which then powers a feed pump for an RO system. However, there is a growing interest in operating seawater desalination systems driven by hydraulic pressure generated directly by wave energy [12, 13].

As the growing population increases demand on the limited global freshwater supply, seawater desalination is an increasingly prominent approach for producing safe drinking water. Research into new desalination membrane technology has been increasing in recent years, resulting in more

robust and less expensive membranes that can be tailored to specific applications [14, 15]. Membranes are made with a variety of organic and inorganic materials and are often first characterized by their pore size or selectivity, with RO membranes having the highest selectivity for ions that enable desalination of seawater and brackish water. These membranes are produced commercially and are typically packaged in a spiral wound module consisting of a flat sheet membrane wrapped around a central tube for the collection of permeate.

Though modern membranes are robust, their performance and longevity are highly dependent on the composition of the feed water and the operating conditions of the system. Poor feed water quality, or lack of pretreatment, can induce chemical and biological fouling, reduce the life of the membrane, and result in poor quality permeate [16]. Permeate water quality is also affected by feed pressure and water recovery; commonly, as feed pressure and recovery increase, less salt mass passes through the membrane and the flow of clean water through the membrane increases.

RO membranes deployed for desalination are conventionally operated with a constant feed pressure or constant flux to facilitate consistent operating conditions and permeate quality [14]. Operating an RO system using only wave motion to drive feed pressure (without pressure dampening) may result in a variable feed pressure that changes with the motion of the waves [17]. The power (P) stored in a wave is directly related to the height (H) and period (T) of the wave [10]:

$$P = \frac{\rho g^2 H^2 T}{64\pi} \quad (1)$$

where g is acceleration due to gravity, and ρ is the density of water. As waves become longer and higher, the power available to pressurize water increases. Depending on the location and time of year, waves can yield between 10 kW and 120 kW per meter of wave height [18]. Clearly, in the ocean's dynamic wave system, feed pressure using only a WEC would not be constant. Because most membranes are designed with constant feed pressure in mind, and because there is no apparent reason for or advantage to operating with variable feed pressure, the effect of such variable pressures on membrane integrity and performance is unknown.

Feed pressure is a major contributor to the net driving force in a membrane system, which is the sum of all the forces responsible for water permeation through the membrane. Feed pressure impacts both the physical integrity of the membrane and many other performance characteristics of RO systems, including permeate flow rate, permeate quality, and recovery. Membrane fouling

mechanisms are different at low and high pressures as well; at higher pressures (and thus higher water flux), RO membrane scaling due to low-solubility minerals is a major concern [16], while at low pressures (i.e., below the osmotic pressure of the feed), osmotic backwashing is a useful method to clean RO and NF membranes [19]. The role that each of these mechanisms play in systems that operate at variable feed pressure is unknown and should be understood to successfully operate such systems.

Literature on variable feed pressure with RO is limited to studies conducted on "pulsed" RO to mitigate concentration polarization effects and improve performance [20-25]. Kennedy et al. [25] tested a variety of conditions and saw a maximum increase of 70% in permeate flow. Abbas and Al-Bastaki modified, validated, and improved the model proposed in Kennedy et al. and demonstrated improved permeate flow and salt rejection afforded by pulsed RO in the form of square and asymmetrical waveform pressure pulses [20, 23, 24, 26]; these results were attributed to the reduction in the effect of concentration polarization [27]. However, in these studies, the focus was on model validation and process optimization, without regard for the impact on membrane integrity over longer periods of operation. Short experiments (30 minutes) using square waves were conducted using either sucrose or 10 g/L NaCl. These studies provide no guidance for potential impacts to membrane integrity that could result from wave-driven variable feed pressure for desalination of seawater.

There has been some modeling of wave-driven desalination systems that include devices like WECs, pressure relief valves, and other energy saving and recovering mechanisms [8, 17, 28]. While these models do consider some of the logistics and economics of implementing such a system, there is no mention of the impact of the variable feed pressure conditions on membrane integrity and long-term performance. There has also been no known pilot-scale assessment of these conditions on RO membranes, even though understanding them is essential to implementing a WDDS. Typical tests for comparing high performance RO membranes are done with a 32 g/L NaCl feed solution at 800 psi (5.5 MPa) and 25 °C [29]. However, in a purely wave-driven system, modeled systems' feed pressure can range from 290 to 1,740 psi (2.0–12.0 MPa) [28]. It is impossible to take performance data from a constant feed pressure test and extrapolate it to apply to such a scenario. Because our water treatment and delivery systems are inherently life-sustaining, it is paramount that their long-term behavior and performance is predictable to a certain degree. For an RO system operating in the open ocean under variable conditions, understanding the impact

on the membrane is germane to performance predictability, particularly if this system is to operate in a developing community with limited resources. Before further development or implementation of a purely wave-driven RO system, there must be fundamental research that considers whether the membrane can handle the dynamics of irregular feed conditions and explores any impact on permeate quality. To investigate the impact of variations in feed pressure on membrane integrity and permeate quality, this research presents results from several experiments with different feed compositions and wave conditions conducted on a commercial RO membrane along with elemental analysis of the product water.

2. Materials & methods

2.1. System construction/flow

A flowchart of the system used to conduct these experiments is illustrated in Fig. 1. Feed water from the feed tank flows by gravity to a pump (Hydra-Cell M03; Minneapolis, MN). The feed water is then pumped through an in-line pressure sensor and heat exchanger to the pressure vessel containing an RO membrane (Dow Filmtec SW30-2540) with an active area of 2.8 m^2. The reject stream flows back to the feed tank through a back-pressure valve, flow meter, and conductivity cell. The permeate stream also flows through a flow meter and conductivity cell back to the feed tank. Feed water temperature is regulated by flowing through a heat exchanger connected to a chiller. Each of the sensors (pressure, conductivity, flow) are connected to a system control and data acquisition system (LabJack; Englewood, CO) to provide visual interface with the experimental setup. The feed pressure sensor was calibrated using an in-line analog pressure gage, and conductivity probes were calibrated with traceable conductivity standards (Fisher Scientific International Inc.; Pittsburgh, PA).

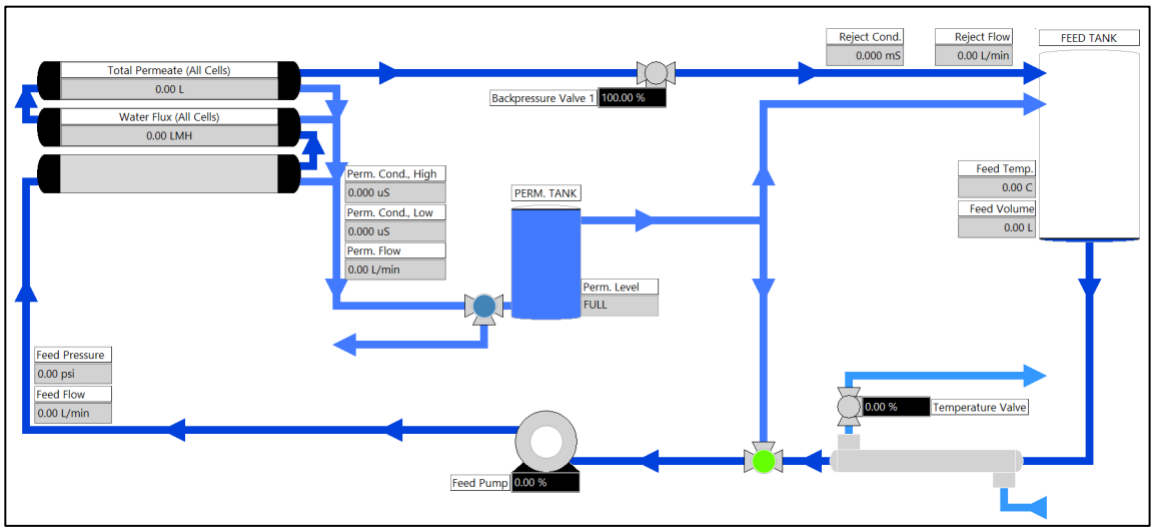

Fig. 1. Flow diagram for the experimental system. Note that the system was equipped with a separate tank to collect permeate, but it was not used for these experiments and permeate was redirected to the feed tank.

2.2. Experimental design

Experiments were of two kinds: wave and integrity. The wave experiments simulated wave motion and were broken down into three regimes: (1) constant flux (J_w = 15 LMH) for 1 hour at the beginning of each experiment, (2) waveform for 7 days, and (3) repeat constant flux for 1 hour at the end. Several experiments were conducted using this basic format with different feed compositions and wave periods. The feed composition for wave experiments included 5–35 g/L NaCl and Instant Ocean (Spectrum Brands Holdings Inc.; Madison, WI), a commercial synthetic seawater blend, with 35 g/L representing seawater salinity. A subset of experiments were conducted with 1.5 times seawater salinity feed prepared with Instant Ocean salt. Integrity tests used 25 g/L NaCl feed held at 650 psi (4.5 MPa) for 2 hours. The integrity tests were performed between wave experiments as a control to monitor any degradation in membrane performance. Table 1 summarizes all the experiments performed. Throughout the experiments with Instant Ocean, permeate samples were collected for water analysis.

Sine-like wave motion was simulated by setting the feed pressure range, wave period, and wave frequency. Guidance on the range of feed pressures was taken from Yu and Jenne [17, 28], which included simulations of a WDDS. Three wave frequencies were used: 1.25 waves/min (48 s wave period), 7.5 waves/min (8 s wave period), and 12 waves/min (5 s wave period). These wave

periods span the spectrum of what might reasonably be experienced near a coastline where a WDDS might operate, and to simulate a system that includes devices such as WECs, pressure accumulators, and pressure relief valves that have the effect of "smoothing" the feed pressure form, as have been present in some simulations [8, 17, 28, 30]. In total, we performed 15 experiments under controlled, sine wave-like conditions. Nine of those were conducted for 7 days, and six were conducted for 24 hours. The latter were performed using a higher frequency of data collection to provide higher data resolution on the differences in performance under three different experimental conditions. Finally, we performed one experiment using feed pressure output from a simulation of a WDDS, using real wave height data from Yu and Jenne [17, 28]. Researchers have developed a numerical model from WEC-Sim, a Matlab-powered time-domain, radiation-and-diffraction-based numerical tool, to evaluate the performance and cost of a WDDS in the United States [17, 28]. The modeled system has several forms, and includes a WEC, a hydraulic accumulator, and a pressure exchanger. Numerically modeled interactions between these components provided feed pressure output to an RO system based on real wave height data from a buoy in northern California. The feed pressure in the model was set to be constrained by the upper limit on operational feed pressure for the modeled membranes, resulting in a waveform with pressure fluctuations between 575 and 800 psi (4.0–5.5 MPa).

2.3. Membrane integrity

The water permeability coefficient A (m s^{-1} psi^{-1}) was the metric used to evaluate whether the membrane integrity had diminished as a result of the wave experiments. This parameter was calculated for each data point according to:

$$A = \frac{J_w}{P_F - \left(\frac{\pi_F + \pi_R}{2}\right)} \quad (2)$$

where J_w is water flux (m s^{-1}), P_F is feed pressure (psi), π_F is osmotic pressure of the feed solution (psi), and π_R is osmotic pressure of the reject (psi). For this calculation, both pressure drop across the membrane (i.e., pressure drop from the inlet to reject) and permeate hydrostatic and osmotic pressure were assumed to be negligible (i.e., $P_{F,out} = P_{F,in}$ and $P_{perm} = \pi_{perm} = 0$). The salt permeability coefficient B (m s^{-1}) was calculated according to:

$$B = \frac{C_p J_w}{\left(\frac{C_F + C_R}{2}\right) - C_p} \quad (3)$$

where C_p, C_F, and C_R are the permeate, feed, and reject stream salt concentration (mg/L), respectively. These concentrations were determined from regressions of concentration vs. conductivity developed for the system. Osmotic pressure of the feed was estimated with the Lenntech web-based calculator, and then π_R was calculated assuming it scaled linearly with conductivity throughout the experiments:

$$\frac{\pi_F}{C_F} = \frac{\pi_R}{C_R} \quad (4)$$

2.4. Analytical procedures

Samples were collected from the permeate stream and analyzed for cations using inductively coupled plasma optical emission spectrometry (PerkinElmer Avio 200 ICP-OES) with an in-house method that was developed to be similar to Standard Method 3120. Samples were analyzed for anions using ion chromatography (Dionex ICS-90) with Standard Method 4110B. Instant Ocean was used as a synthetic seawater; the blend includes B, Ca, K, Mg, Na, and Sr at concentrations intended to be close to those found in seawater. Samples were collected from the permeate stream during the start and end constant flux periods, and throughout the wave phase. The samples collected during the wave phase were collected over the duration of one full wave and were homogenized before being placed in a sample container and analyzed for major cations (B, K, Na, Ca, Mg, and Sr) and select anions (Cl, Br, and SO_4). The average feed solution composition for these analytes is summarized in the supporting information in Table SI-1.

2.5. Data processing procedures

Data were retrieved from the experimental setup as .csv files, imported into Matlab (version R2019a, The MathWorks Inc., Natick, MA), and processed using an application developed in-house. The application calculated osmotic pressures from measured feed conductivity, which then calculated other values such as the salt and water permeability coefficients (Eqs. 2-4). Simple functions were used to calculate mean and standard deviation values over run time durations that

corresponded to either a constant flux period or a wave period. Initial startup and ramp-up portions of each experiment were not included in these calculations. In some cases, instrument noise caused calculated value data points (i.e., data points that were not measured but rather calculated *a posteriori*, such as the water permeability coefficient) to have significant deviation (> 10x) from expected values based on the data points immediately before and after. When this was the case, the Matlab *find* function was used with logic to exclude these from calculations of descriptive statistics.

3. Results & discussion

3.1. Membrane performance and integrity under wave conditions

3.1.1. Sine waves

The average and standard deviation for pressure, flux, temperature, permeate conductivity, salt rejection, water permeability coefficient, salt permeability coefficient (B), and percent recovery are summarized in Table 1 for the 7-day experiments. These values represent the average of data points collected every minute for the duration of the experiment. The system was set to maintain a temperature of 19–20 °C, and the average across all experiments in Table 1 was 19.7±0.6 °C. Pressure for each experiment is the average of the high- and low-pressure settings of the sine wave; for these experiments, the waves were sinusoidal, and the system spent an equal amount of time ramping up and down to the peak and trough of the regular wave motion. Flux, permeate conductivity, water permeability coefficient, salt permeability coefficient, and recovery averages for each experiment changed, as expected, with changes in feed salinity and pressure settings (e.g., E3 resulted in lower average flux due to higher feed salinity despite otherwise identical operating conditions to E2) and signal no obvious membrane damage from the waves (differences due to variations in wave frequency are discussed later). Not surprisingly, the standard deviation on these performance parameters is larger than those for integrity tests owing to the variation in the feed pressure.

Table 1. Condition, pressure, flux, temperature, permeate flow, permeate conductivity, salt rejection, water permeability coefficient (*A*), salt permeability coefficient (*B*), and percent recovery for sine wave experiments conducted for 7 days.

Conditions	Designation	Pressure (psi)	Pressure (MPa)	Flux (LMH)	Temp. (°C)	Perm. Flow (L min^{-1})	Perm. Cond. (µS cm^{-1})	Salt Rej. (%)	*A* (m s^{-1} psi^{-1})	*B* (m s^{-1})	Recovery (%)
5 g/L NaCl 200-500 psi 7.5 wave/min	E2	350±120	2.41±0.83	25.6±10.0	19.3±0.3	1.1±0.4	30±3	99.7±0.0	$2.6±0.2×10^{-8}$	$1.4±0.7×10^{-8}$	21.0±5.8
20 g/L NaCl 200-500 psi 7.5 wave/min	E3	360±110	2.48±0.76	10.1±7.5	19.1±0.4	0.5±0.3	400±60	98.9±0.2	$2.6±0.1×10^{-8}$	$2.3±1.9×10^{-8}$	8.5±5.5
35 g/L NaCl 500-900 psi 7.5 wave/min	E4	720±150	4.96±1.03	18.4±9.3	19.5±0.3	0.8±0.4	865±75	98.6±0.1	$1.8±0.4×10^{-8}$	$5.9±3.0×10^{-8}$	12.9±5.1
35 g/L NaCl 500-900 psi 1.25 wave/min	E5	710±150	4.89±1.03	18.5±8.4	20.3±0.4	0.8±0.4	550±60	99.1±0.1	$1.8±0.3×10^{-8}$	$3.5±1.8×10^{-8}$	12.5±4.8
35 g/L NaCl 500-900 psi 12 wave/min	E6	710±140	4.89±0.97	18.4±10.1	19.2±0.1	0.8±0.5	785±105	98.7±0.2	$1.9±0.6×10^{-8}$	$3.7±2.7×10^{-8}$	11.4±5.1
Instant Ocean 500-900 psi 7.5 wave/min	E7	680±170	4.69±1.17	24.3±11.3	20.2±0.4	1.1±0.5	415±45	99.1±0.1	$2.6±0.6×10^{-8}$	$4.4±2.1×10^{-8}$	16.0±5.4
Instant Ocean 500-900 psi 1.25 wave/min	E8	700±140	4.83±0.97	24.5±8.6	20.2±0.3	1.1±0.4	250±30	99.5±0.1	$2.6±0.6×10^{-8}$	$2.7±1.1×10^{-8}$	16.6±3.8
Instant Ocean 500-900 psi 12 wave/min	E9	700±150	4.83±1.03	23.4±10.6	20.4±0.2	1.1±0.5	300±15	99.4±0.0	$2.6±0.6×10^{-8}$	$3.0±1.3×10^{-8}$	15.8±5.2
1.5× Instant Ocean 500-900 psi 7.5 wave/min	E12	700±150	4.83±1.03	13.2±8.9	20.3±0.5	0.6±0.4	740±95	98.9±0.1	$2.9±1.7×10^{-8}$	$3.1±2.1×10^{-8}$	8.2±4.8

Comparing all nine of these experiments to one another is not sensible owing to their different feed conditions, but for those experiments with identical feed salinity and waveform pressure ranges (e.g., E4-E6 and E7-E9), we can examine the impact that wave frequency had on performance. In experiments with the same feed, there is almost no difference between different wave frequencies with respect to water flux (average of 18.5 LMH for 35 g/L NaCl and 24.1 LMH for Instant Ocean) or water recovery (average of 12.3% for 35 g/L NaCl and 16.1% for Instant Ocean).

It is difficult to compare the results of these experiments to the typical operating parameters of full-scale desalination plants because there are no full-scale plants that use variable feed pressures at this magnitude and frequency (closed-circuit desalination systems are a possible exception, though the pressure swings are less dramatic and happen over the course of a few hours rather than seconds, as in this study [31]). Nevertheless, it is worth comparing these results to what is typical for seawater desalination plants. The results presented in Table 1 for the wave experiments compare favorably to the performance of full-scale desalination plants.

Conventional seawater desalination plants that use a single stage and single pass configuration operate with a flux of 12–17 LMH between 800–1,100 psi (5.5–8.0 MPa) and achieve recoveries of up to ~ 50% with permeate total dissolved solids (TDS) < 500 mg/L [32, 33]. Desalination systems using hydrokinetic energy have reported recoveries of 33–37% [9]. Recoveries were lower in these experiments but would increase with an increased operating pressure range and additional membrane elements in the array; however, this would also increase the specific energy consumption of the system and might not be achievable with a purely wave-driven desalination system [33]. Wave-driven feed pressures as high as 1,800 psi (12.4 MPa) were achieved in simulations done by Yu and Jenne [28] of a system without hydraulic accumulators or pressure relief valves, but were confined to 725–870 psi (50–60 MPa) when these components were included. In a separate analysis, their desalination model targeted 70 ppm TDS permeate quality with a higher targeted feed pressure of 1,000 psi (6.9 MPa) [17]. However, targeting the higher recoveries seen in conventional RO plants may not achieve the best results. Folley et al. [8] simulated a wave-driven RO plant that used a pressure exchanger-intensifier to facilitate a maximum recovery of 25%. Analysis of the results showed that higher recovery by using more membranes resulted in lower quality permeate and diminishing returns for recovery while increasing the specific energy consumption. While these results reflect a special configuration of

a simulated system, with better understanding of the variable feed pressure on membrane integrity a deployed system could be optimized to produce conditions that protect the integrity and longevity of the membrane while also producing high quality permeate. Additionally, achieving higher pressures and efficiencies in a purely wave-driven system would be highly dependent on local wave conditions.

Water permeability coefficient, salt permeability coefficient, and permeate conductivity are shown in Fig. 2 for the beginning and ending constant flux periods of the 7-day experiments. The approach taken for these experiments was to gradually change experimental conditions, initially keeping salinity low (5 g/L NaCl) and maintaining the same wave frequency (7.5 wave/min) before gradually increasing the salinity and wave pressure and varying the wave frequency. As shown in Fig. 2, there was no significant change in average water permeability during the wave phase of the experiments. There was a decrease in average water permeability with increasing feed concentration due to the increased pressure needed to maintain constant flux. Likewise, the salt permeability and permeate conductivity did not change considerably between the beginning and end of each 7-day experiment and tracked as expected with changes in feed salinity. An exception to this is the results from the 7.5 wave/min experiment conducted with 35 g/L NaCl. Permeate conductivity (and salt permeability coefficient) were observed to increase over the course of the experiment; this is reflected in the results in Fig. 2. This result is not consistent with the other results, which show no significant change in these parameters from the beginning to the end of the experiment. There is no noticeable trend in these parameters with respect to changes in wave speed from experiment to experiment; the only observed changes occur with a change in feed composition.

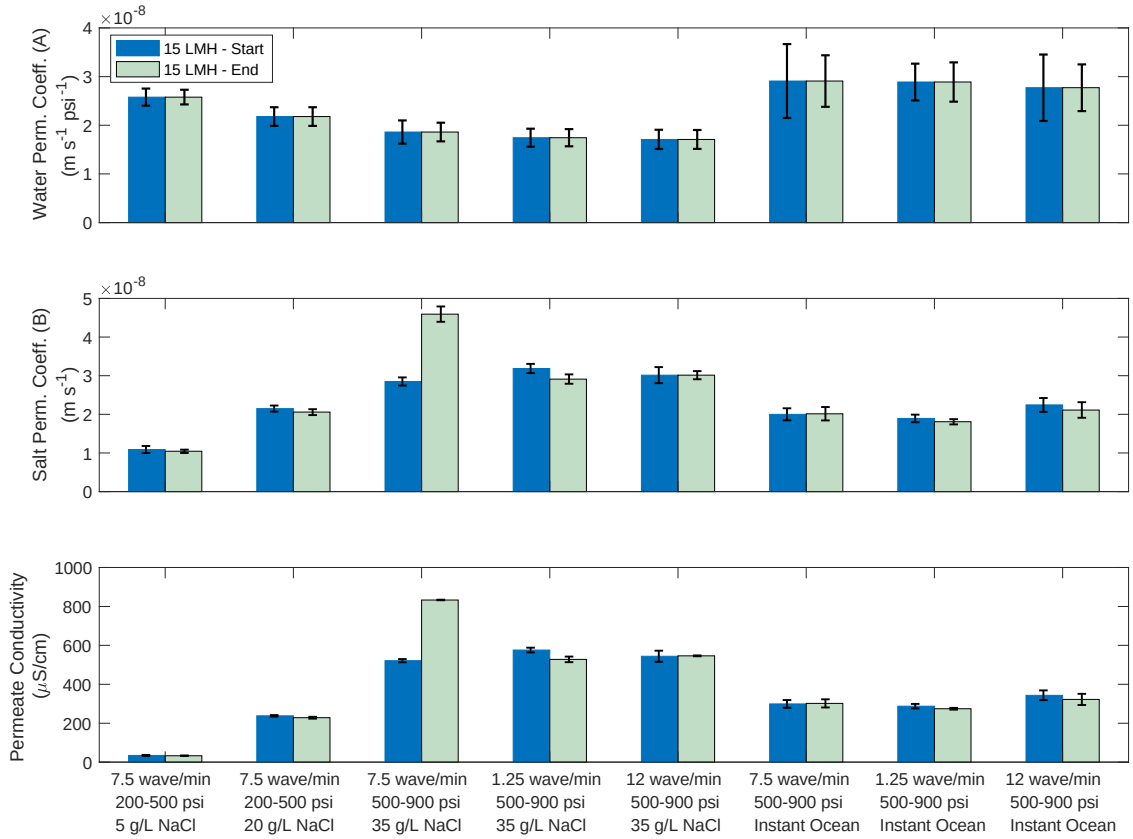

Fig. 2. Water permeability coefficient (*A*, top frame), salt permeability coefficient (*B*, middle frame), and permeate conductivity (bottom frame) for the beginning and ending constant flux periods for each sine wave (7-day experiment).

The pressure (top frames, red), flux (middle frames, blue), and permeate conductivity (bottom frames, green) are shown in Fig. 3 for a representative 0.1 hour of operation for the three wave conditions. The purple line on the pressure and flux plots represents the average pressure and flux, respectively, for these experiments. The plots show the variation in permeate quality and flux that can result from different wave conditions. Waves at 1.25 wave/min produced flux between 10.1–38.1 LMH and permeate conductivity between 330–405 µS/cm; 7.5 wave/min between 7.5–43.3 LMH and 425–440 µS/cm; and 12 wave/min between 6.8–39.7 LMH and 515–530 µS/cm. In each plot, the observed double hump is the point at which the system restarted the wave cycle. When the cycle restarted, the system sustained a higher pressure for longer, resulting in the permeate conductivity dips observed for all three wave conditions. The longest period waves (1.25 wave/min, E5 and E8) produced the lowest conductivity permeate (overall averages from Table 1 of 550±60 µS/cm and 250±30 µS/cm, respectively) but also the widest fluctuations in permeate

quality, while shorter waves produced lower quality permeate with smaller fluctuations. For both feed compositions (Instant Ocean and 35 g/L NaCl), the mid wave frequency of 7.5 wave/min (E4 and E7) resulted in the highest average permeate conductivity (overall averages from Table 1 of 865±75 µS/cm and 415±45 µS/cm, respectively) within each group. The permeate conductivity for those experiments with the shortest period (12 wave/min, E6 and E9) fell in between (overall averages from Table 1 of 785±105 µS/cm and 298.8±15.0 µS/cm, respectively). Based on the system described by Yu and Jenne and the results of their simulations [15, 25], the pressure profile from an actual system might be closer to that for the slower waves in these sine-like experiments. In other words, an actual system may have longer periods of sustained high and low pressure better represented by the 1.25 wave/min experiments rather than sharp pressure pulses of the 7.5 and 12 wave/min experiments. This is demonstrated to some degree by the experiments with the more "random" wave profile shown in Fig. 5 and discussed later (full profile shown in Fig. SI-1). Thus, while the significant variability in permeate conductivity observed for the slower waves (and to a lesser extent in the faster waves) is an important phenomenon to consider in future experimentation, the current dataset presented here is not adequate to explain these variations.

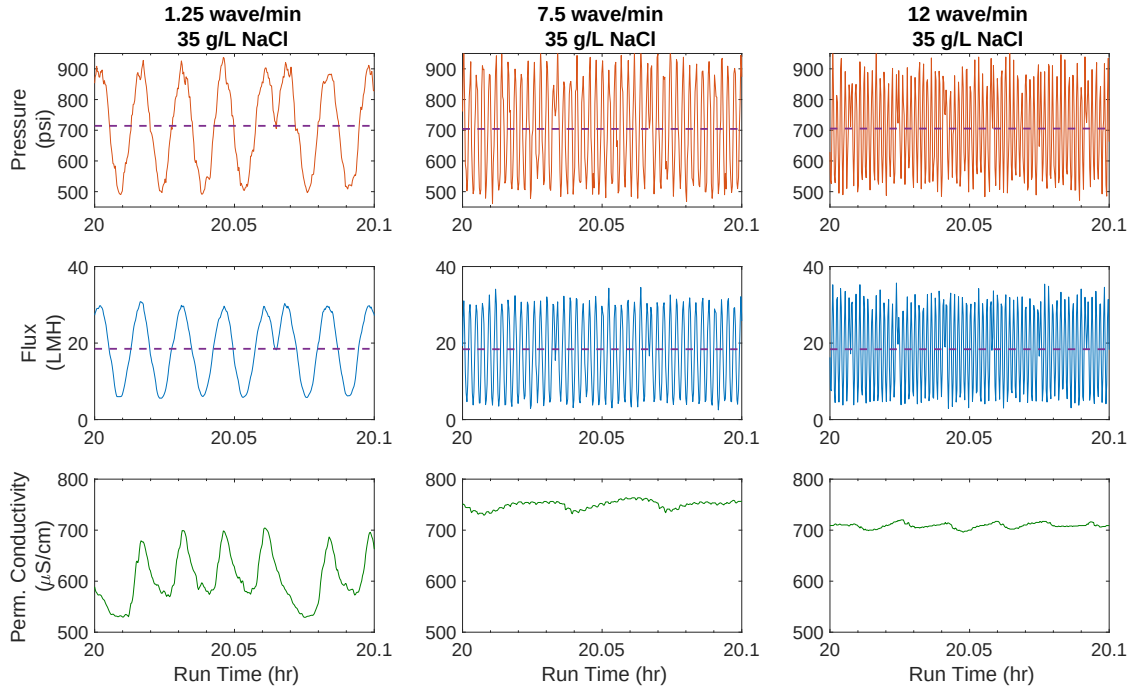

Fig. 3. Pressure, flux, and permeate conductivity over 0.1 hr of run time for experiments with 1.25 wave/min (left frames), 7.5 wave/min (middle frames), and 12 wave/min (right frames).

These results show the impact that sea conditions could have on permeate water quality and highlight how low-pressure swings can cause major swings in permeate quality. Lower permeate conductivity in the longest wave period can be interpreted through the relationship between power generated per unit wave crest (p), wave height (H), and wave period, as described in the introduction, and approximated as $p = 2H^{2.5}$ [34]. Thus, sea conditions with waves with longer periods may result in more powerful waves that could generate a higher feed pressure for an RO system. In simulations of wave-driven RO done by Yu and Jenne [28], wave environments with higher periods and higher significant wave heights yielded higher recoveries and lower permeate concentrations. In their simulations, hydraulic accumulators and pressure relief valves were included to modulate the feed pressure between the designed operation range for the membrane (610–825 psi / 4.2–5.7 MPa). When the pressure exceeded this range, these components had the effect of holding feed pressure constant at the high end of the range until wave height lowered and the pressure fell. This high wave energy simulation environment is most akin to the longest waves modeled in this research (1.25 wave/min, E5 and E8 in Table 1) because those simulations held the highest pressure constant for an extended period of time. Similarly, the shorter waves (7.5 wave/min and 12 wave/min; E4, E6, E7, and E9 in Table 1) more closely resemble the lower energy wave environments from those simulations. Each of the wave experiments in this research produced water with estimated TDS <350 mg/L, but these results, coupled with those in Yu and Jenne [28], highlight the impact that ocean conditions can have on this type of RO system. Further, the results shed light on possible complications of trying to deploy a WDDS due to the dependence on local wave conditions.

3.1.2. Variable feed composition

The first 24 hours of two separate experiments conducted under identical wave conditions (7.5 wave/min, 500–900 psi / 3.45–6.2 MPa), but different feed compositions, are shown in Fig. 4. These 24-hour periods include the initial 15 LMH constant flux period followed by the waveform. The left two panels show the flux and permeate conductivity for a feed with Instant Ocean, with averages over the wave portion (i.e., t = ~1.5–24 hr) of 25.7±10.4 LMH and 415±45 µS/cm, respectively. The right two panels show the flux and permeate conductivity for a feed of 1.5× seawater salinity made with Instant Ocean salt, with averages over the wave portion of 13.5±9.2 LMH and 940±90 µS/cm, respectively. For both experiments, coming out of the constant flux

period causes the permeate conductivity to change with the feed pressure. For the experiment with 1.5× Instant Ocean, this causes an initial rise in permeate conductivity because the pressure needed to hold 15 LMH at this concentration (740±35 psi / 5.1±0.25 MPa) is higher than at the beginning of the wave experiment (500 psi / 3.45 MPa). Thus, there is a brief period of osmosis, causing increased permeate conductivity as the system adjusts to these conditions. During the wave portion of these experiments, membrane performance parameters stayed consistent. While this is a result of the operation of this system, it also provides insight into the large changes in permeate quality that could occur with the large pressure swings that could happen in a deployed system as the feed pressure varies with sea conditions. For each experiment, there was a period after switching from constant flux to wave mode where permeate conductivity would adjust to the wave conditions, but after reaching a steady state point, it did not change dramatically for the remainder of the experiment.

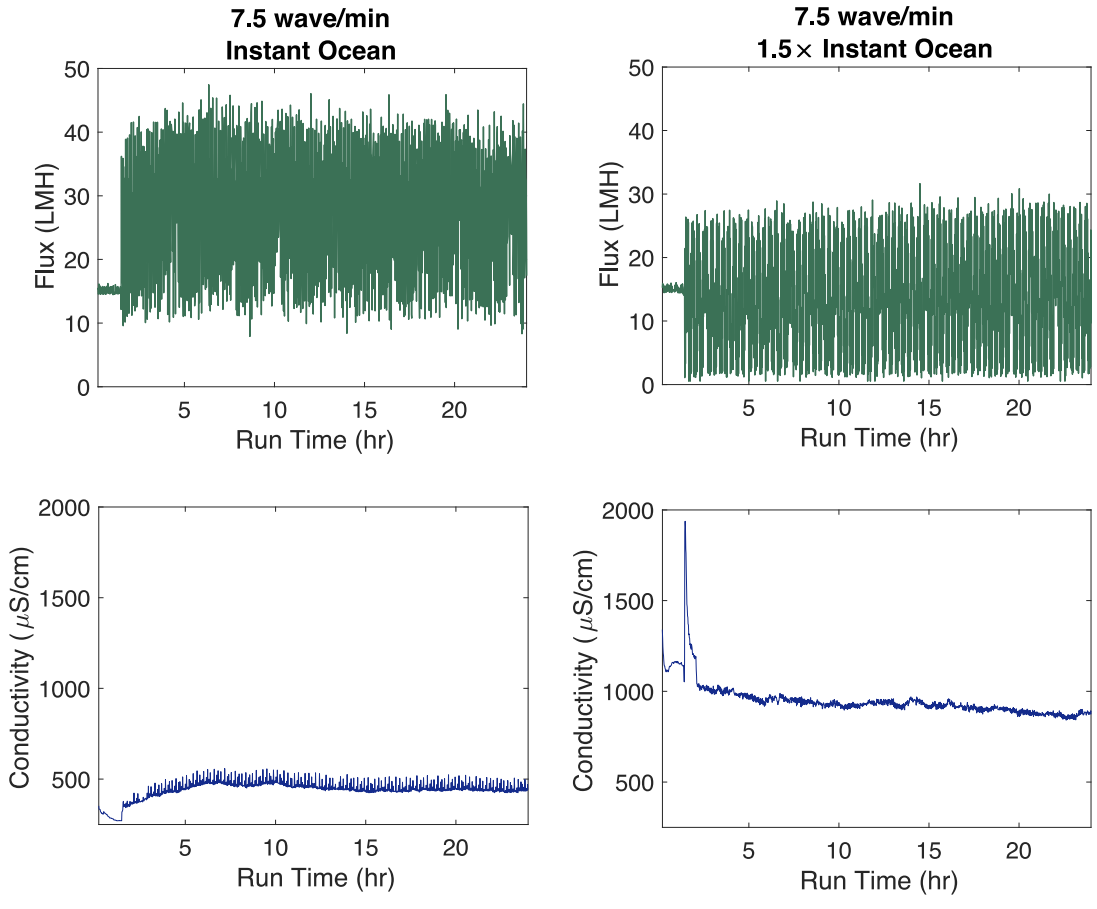

Fig. 4. Permeate flux and conductivity as a function of time for the first 24 hours of experiments conducted at 500–900 psi (3.45–6.20 MPa) and 7.5 wave/min with Instant Ocean (left frames) and 1.5× Instant Ocean (right frames).

The nature of the wave at these higher feed concentrations has a negative effect on permeate conductivity. The osmotic pressure of the 1.5× Instant Ocean feed is estimated to be 575 psi (4.0 MPa). Because this is larger than the lowest pressure of the wave (500 psi / 3.45 MPa), there is osmosis of water (i.e., water moving from the permeate to the feed side of the membrane) during the trough of the wave, causing an increase in permeate conductivity. Conversely, at the highest pressure of the wave (900 psi / 6.2 MPa), water flux increases, diluting the permeate and bringing the conductivity down. Dipping into osmosis with lower feed pressures has been recently explored as a method for membrane backwashing to remove some scale from the membrane surface [35, 36], but the impact of doing this frequently is unknown. In a deployed system, this should be avoided to improve the quality of the permeate water, as the permeate conductivity is much higher in the experiment with concentrated seawater. In these controlled wave conditions, permeate conductivity is somewhat balanced by the peak and trough of the wave, but the more chaotic nature of actual wave conditions would cause significant variation in permeate quality, as shown in Fig. 3 and in the simulations done by Folley et al. [8] and Yu and Jenne [28].

The experimental conditions depicted in Fig. 4 are an approximation of conditions in a multistage configuration for a WDDS. Assuming a multistage single-pass configuration, and assuming that feed pressures are the same in each stage due to wave motion, then as the feed pressure goes below the osmotic pressure of the feed solution, there will be a detriment to permeate quality. Further complicating this multistage scenario, the osmotic pressure of the feed for any stage after the first will not be constant, because like the permeate salinity, reject salinity varies with wave motion. This is in contrast to conventional multistage configurations operating under constant pressure, where the feed for the second stage would be predictable and constant. In theory, it is possible to amplify applied wave pressure in subsequent stages to avoid this effect, but it might require more sophisticated equipment to implement, thus increasing cost, operating difficulty, and system size, and detracting from the potential of a WDDS to be deployed in coastal developing communities. Previously mentioned models [8, 28] that simulate a similar system assume single-pass configurations; thus, it is unclear how a multi-pass configuration might affect system design and operational efficiency.

One reason often given for including multiple stages is that it will increase recovery, thus reducing the volume of brine that needs to be disposed and reducing disposal costs [33], which can account for 5–33% of the total cost of the process [37]. Brine streams contain high concentrations of dissolved solids and pretreatment chemicals, if they are used, and there are negative environmental effects associated with each brine disposal method [37]. Most likely, a WDDS would be situated near the WEC (e.g., on the seabed), so the most suitable method for brine disposal would be to discharge directly in the surrounding ocean. Much of the cost associated with brine disposal is transport to the disposal site, typically from a distant location [37]. In this regard, the cost of brine disposal for a WDDS would be limited to the nominal cost of piping infrastructure needed to carry the brine a sufficient distance from the RO intake. The cost of the brine disposal approach should be weighed against the cost of adding membrane elements and other system components necessary to increase recovery. Provided that the permeate is of sufficient quality, it is possible that this cost will be higher than the additional brine disposal associated with lower recovery and a less complicated system overall.

A critical aspect to consider in potentially deploying a WDDS is the cost of pretreatment. Poor influent water quality can cause membrane fouling and scaling, leading to a shorter membrane lifetime, high maintenance costs, and deteriorating system performance [38]. The synthetic feed solutions in these experiments were prepared with only sea salts and lab-grade deionized water, so the results reflect operation with high feed water quality. Because the entirety of the influent flow is pretreated but only a fraction is recovered, some of the cost of pretreatment is wasted along with the brine stream. The results presented here are encouraging for the capacity of membranes to handle the stress of oscillating pressure, but the economic viability of a full-scale WDDS, including pretreatment, is unclear. Further, a better understanding of the dynamics of membrane fouling and scaling in a WDDS would need to be more fully understood before making such a value judgement.

3.1.3. Random wave conditions

The feed pressure, flux, and permeate conductivity for one cycle of a randomly generated waveform are shown in Fig. 5. A plot of the targeted waveform obtained from NREL is shown in the supporting information in Fig. SI-1. Further details of the modeled system are available in Yu and Jenne's publication [28]. The feed pressure output from the model used in this experiment was

a total of 50 minutes that was looped over itself continuously for 14 days. Dotted lines on each plot represent the average value for the entire experiment. Average flux was 21.7±3.1 LMH, pressure was 730±60 psi (5.0±0.4 MPa), and permeate conductivity was 460±30 µS/cm—similar to the values for the sine-like wave experiments (see Table 1). The water permeability constant was $2.1\pm0.3\times10^{-8}$ m s^{-1} psi^{-1} (again, similar to that of the sine-like wave experiments), while recovery and salt rejection were 24.1±2.4% and 99.0±0.1%, respectively.

Despite the slightly lower average water permeability constant, recovery in this experiment was markedly higher than in the previous experiments conducted with Instant Ocean. This is likely due to changes in system backpressure valve settings, which resulted in different feed flow rates in the experimental system that aided the system in more accurately reproducing the higher degree of randomness in this waveform (compared to the simple sine wave from previous experiments). Permeate conductivity shows a similar relationship to feed pressure, as we saw in the longest sine-like waves (1.25 wave/min), and was much more variable than what was seen with longer waves (7.5 and 12 wave/min; see Fig. 3). During times of higher pressure (e.g., around t = 100.1 hr in Fig. 5), we see higher flux and thus higher permeate flow, causing permeate conductivity to decline. When the system experiences the sudden drop in pressure seen around this time, permeate conductivity rises as permeate flow decreases. In this plot, permeate conductivity swings by approximately 100 µS/cm, which corresponds to a change in TDS of ~80 mg/L. These permeate quality results are consistent with simulations done by Folley et al. [8] and Yu and Jenne [28], thus providing some experimental validation to these model results. Folley et al. presented a model with product water salinity of 200–400 ppm and feed pressure of 550–800 psi (3.8–5.5 MPa), very similar to the experiments conducted here (though their model was for a system with 165 membranes). Yu and Jenne used a pressure range of 610–810 psi (4.2–5.7 MPa) in their model with 183 membranes, producing water with 120–380 ppm salinity (depending on sea state). In these models, researchers assigned a maximum pressure at which to engage the pressure relief valve on their modeled systems.

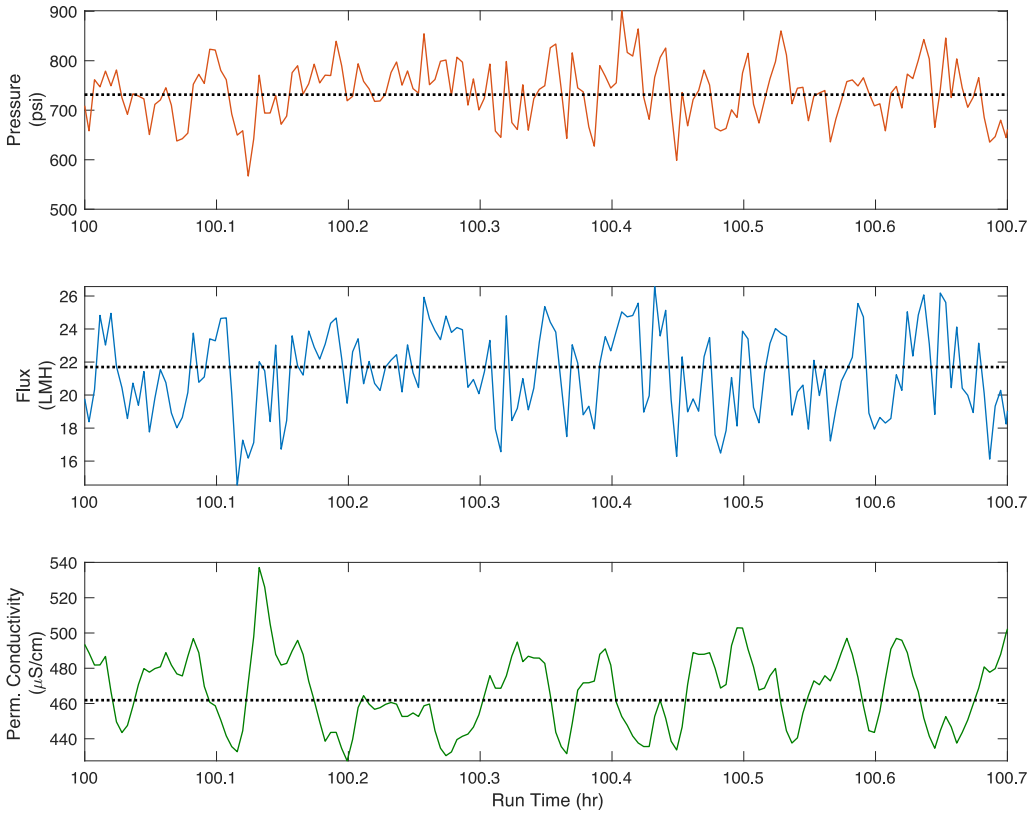

Fig. 5. Pressure (red line, top frame), flux (blue line, middle frame), and permeate conductivity (green line, bottom frame) for one cycle (approximately 50 minutes) of a randomly generated waveform.

While many membranes are assigned a maximum operating pressure, this is assumed to be for continuous, not intermittent, operation. The commercial membrane used in our experiments (Dow Filmtec SW30-2540) has a maximum operating pressure of 1,000 psi (6.9 MPa). However, several experiments were cut short when the system caused a pressure spike to > 1,100 psi, with no apparent damage to the membrane. It would be useful to better understand the upper limits of pressure that membranes can acutely sustain, as this could produce a product water with lower salinity. Higher feed pressures typically result in higher quality permeate, so allowing for times with higher peak pressure during system operation could balance out the times when the sea state is calmer and producing lower feed pressures and saltier permeate.

3.2. Membrane integrity

The water permeability coefficient, flux, and salt rejection, averaged over the last hour of each integrity test and plotted against the total wave time at each point, are shown in Fig. 6. The total wave time is the total number of hours that the membrane was subject to wave-like conditions up until that integrity test. These experiments were conducted between wave tests to evaluate membrane integrity under identical conditions. Data was collected once every 60 seconds during these integrity tests, so each point in Fig. 6 represents the average and standard deviation of 3,600 data points. The membrane was subject to a total of 1,770 hours of wave action, and the water permeability coefficient showed no appreciable change after membrane compaction in each integrity test. The water permeability coefficient was initially $2.1\times10^{-8}\pm0.1\times10^{-8}$ m s^{-1} psi^{-1} for compaction and dropped 7.4% to $2.0\times10^{-8}\pm0.2\times10^{-8}$ m s^{-1} psi^{-1} by the last integrity test. There was a more significant drop in flux, with compaction at 28.3± 0.9 LMH and a drop of 18.4% to a low of 23.0±0.8 LMH. Salt rejection stayed > 99% for all integrity tests except one, in which it dropped to 98.9%.

A decline in flux over time has been previously associated with membrane fouling [39-41] in experiments with constant feed pressure. While the results in Fig. 6 are from experiments at constant pressure, the wave experiments conducted under similar feed and wave conditions show no significant decline in average flux (see Table 1). Instead, this flux decline could be attributable to continuing membrane compaction after the initial compaction procedure, as feed compositions and feed pressures increased with each experiment. Indeed, we see a large dip in flux for the first three integrity tests, after which it is more consistent between each consecutive integrity test. These results present further evidence that membrane integrity and performance were not impacted to a large degree by the variable feed pressure experiments described in section 3.1.1 and 3.1.3.

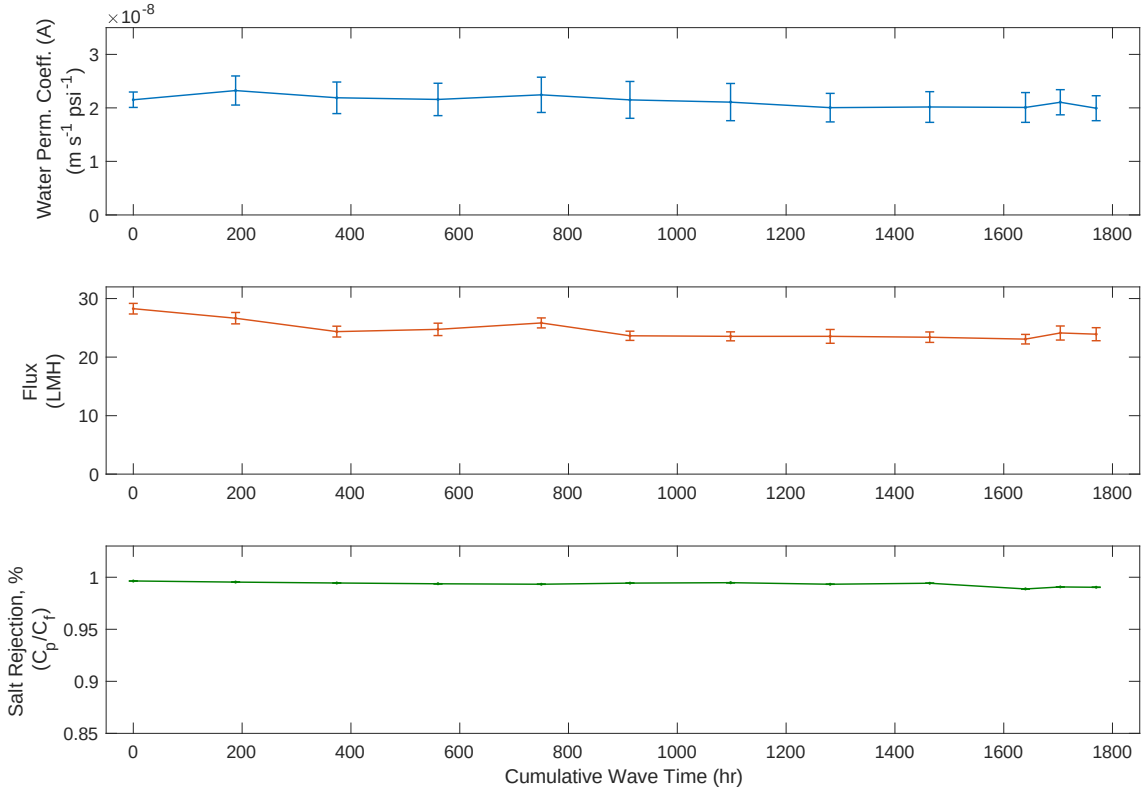

Fig. 6. Water permeability coefficient (*A*, top frame), flux (middle frame), and salt rejection (bottom frame) for integrity tests conducted between each wave experiment.

Deteriorating water flux is typically associated with some form of membrane fouling, be it biological, organic, inorganic, or particulate/colloidal in nature [41]. The degree to which concentration polarization impacts these results is also unclear. Concentration polarization occurs under steady operating conditions when the concentration of solutes is higher in the immediate vicinity of the membrane surface in the feed channel. This causes precipitation of solutes on the membrane surface, inducing fouling, reducing water flux, and lowering the permeate quality [41]. This phenomenon is typically observed under steady operating conditions, but has never been studied under the variable flow conditions described in these experiments. It is possible that the constant variations in cross-flow velocity due to variable feed pressure cause sufficient mixing in the feed channel to mitigate some of the deleterious effects of concentration polarization. Ramakul et al. [42] found reduced concentration polarization in experiments with pulsed flow periodic operation of hollow fiber-supported liquid membranes for the separation of lanthanide metal. The proposed mechanism was a disturbance in the boundary layer between the feed solution and membrane by variations in flow. Similar results and rationale were published by Kennedy et al.

[25] who observed increased permeation rates with pulsed flow over non-pulsed flow; this effect was stronger with a higher frequency of pulses. Comparable results have been obtained and modeled by others as well [20, 21, 23, 24, 26]. Therefore, it is possible that varying pressure in this manner reduces the fouling effects of concentration polarization. Though this is not a primary objective of wave-driven RO, it is a valuable side effect that warrants additional examination in later experiments.

3.3. Cation and anion rejection in permeate

The rejection efficiencies for cations are shown in Fig. 7 for the three wave periods studied with Instant Ocean, and the rejection efficiencies for Cl and Br are shown in Fig. 8 for the same sets of experiments. Cation and anion rejection results for the experiment using the NREL waveform (section 3.1.3) are presented in the SI as Figs. SI-2 and SI-3. These results are not markedly different from those presented in Figs. 7 and 8, highlighting the ability of a WDDS to achieve high rejections under varied conditions. Of the nine experiments conducted for 7 days, four were conducted with Instant Ocean. Boron was rejected at a lower rate than other cations. The average rejection during the constant flux periods was 85.8±2.5% and 88.4±0.6% for the wave periods. The higher average rejection during the wave phase can be explained by the higher pressures experienced during these periods, as boron rejection is higher at higher pressures [43, 44]. No significant decreases in boron rejection were observed between the starting and ending constant flux periods. The largest observed difference was a 2.6% increase during the constant flux periods for the 7.5 wave/min experiment, reflecting a permeate boron concentration decrease of 0.1 mg/L. Boron rejection was also not markedly different as a result of wave frequency. The average of the three wave samples for the 7.5, 1.25, and 12 wave/min experiments was 88.5±0.7%, 88.1±0.8%, and 88.7±0.3%, respectively.

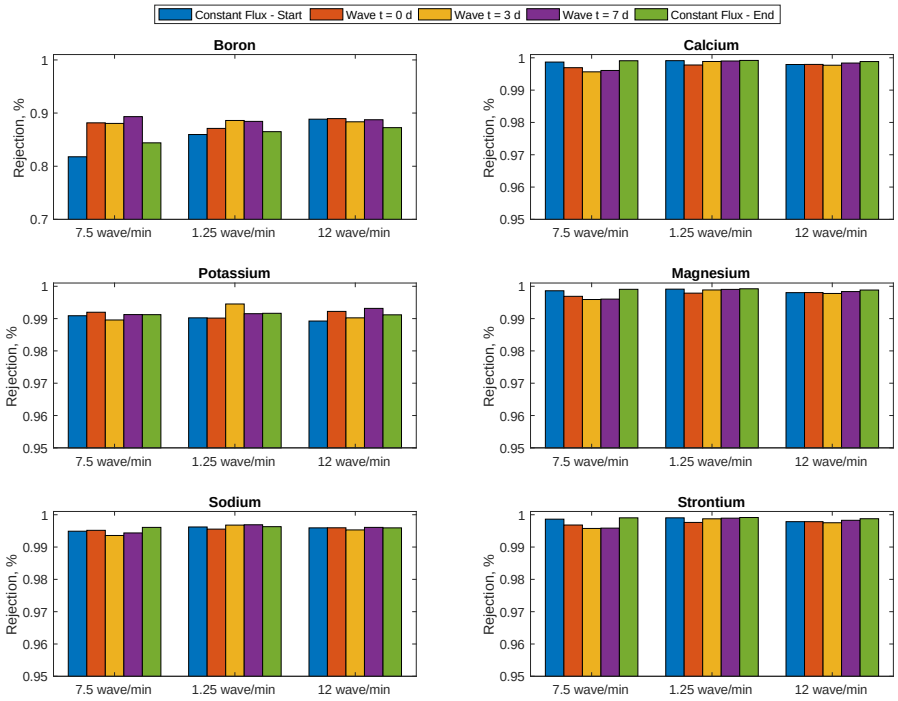

585

586 **Fig. 7.** Rejection efficiencies for B, Ca, K, Mg, Na, and Sr for experiments conducted with Instant
587 Ocean.
588

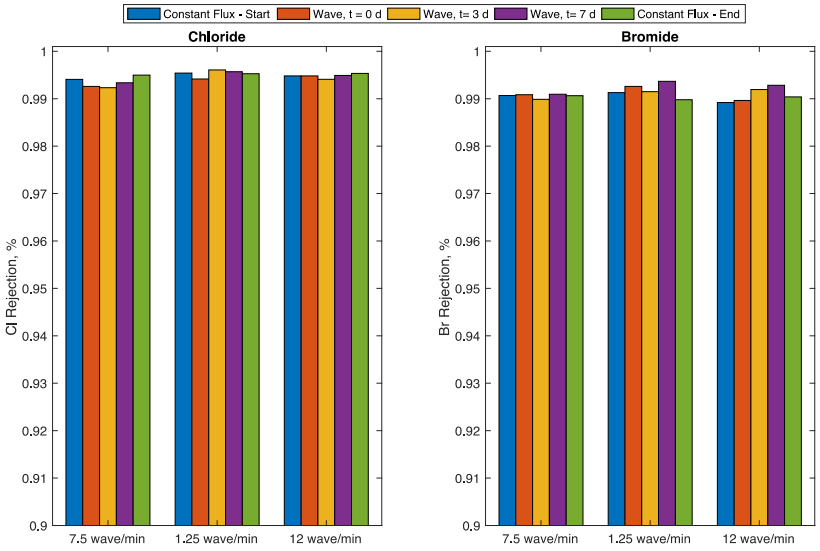

589

590 **Fig. 8.** Rejection efficiencies for Cl and Br for experiments conducted with Instant Ocean.
591

592 Rejections of divalent cations (Ca, Mg, Sr) were slightly higher than those of monovalent
593 cations (K, Na), as is expected. Rejection was 99.0–99.6% for K and Na during both the constant
594 flux and wave phases. For divalent cations, rejection was 99.6–99.8% throughout the entirety of

each experiment. These results show that the variable feed pressure due to the simulated waves was not a detriment to membrane performance and that the membrane performed as might be expected under constant feed pressure conditions. Cl and Br rejection were high, as would be expected under a constant pressure operating condition. Average rejection for Cl was 99.5% and for Br was 99.1%. Tables SI-2 and SI-3 in the supplemental information contain the average concentration for each of these elements for both the constant flux phase and the wave phase, as well as the WHO guideline concentrations for drinking and irrigation water, where available. The permeate concentrations for each element for all experiments with Instant Ocean met these guidelines, but the experiment with concentrated Instant Ocean exceeded the drinking water guidelines for boron and sodium.

The cation rejections for the experiment conducted with 1.5× Instant Ocean are shown in Fig. 9, and anion rejections are shown in Fig. 10. Cation and anion rejection were consistent throughout the experiment. The trend is similar to those experiments conducted with normal concentration: boron had the lowest rejection (81.5±1.1%) followed by the monovalent cations (K and Na > 98.7%) and then the divalent cations (Ca, Mg, and Sr > 99.2%). Br rejection averaged 98.5% and Cl rejection averaged 98.9%. Lower rejections overall can be attributed to the higher salinity feed used for this experiment. The lower rejection observed for all elements for the t = 0 d wave sample (Fig. 9, red bar) can be attributed to the surge in permeate conductivity observed after the system was switched from constant flux mode to wave mode (see bottom right panel, Fig. 4). This sample was collected for each experiment within minutes of making the switch from constant flux to wave mode, so it was likely collected during that period the permeate conductivity surged. There was no ending constant flux period due to experimental system failure (not membrane failure), so we cannot make any comparison, though there is no clear decline in rejection for either cations or anions over the course of the experiment.

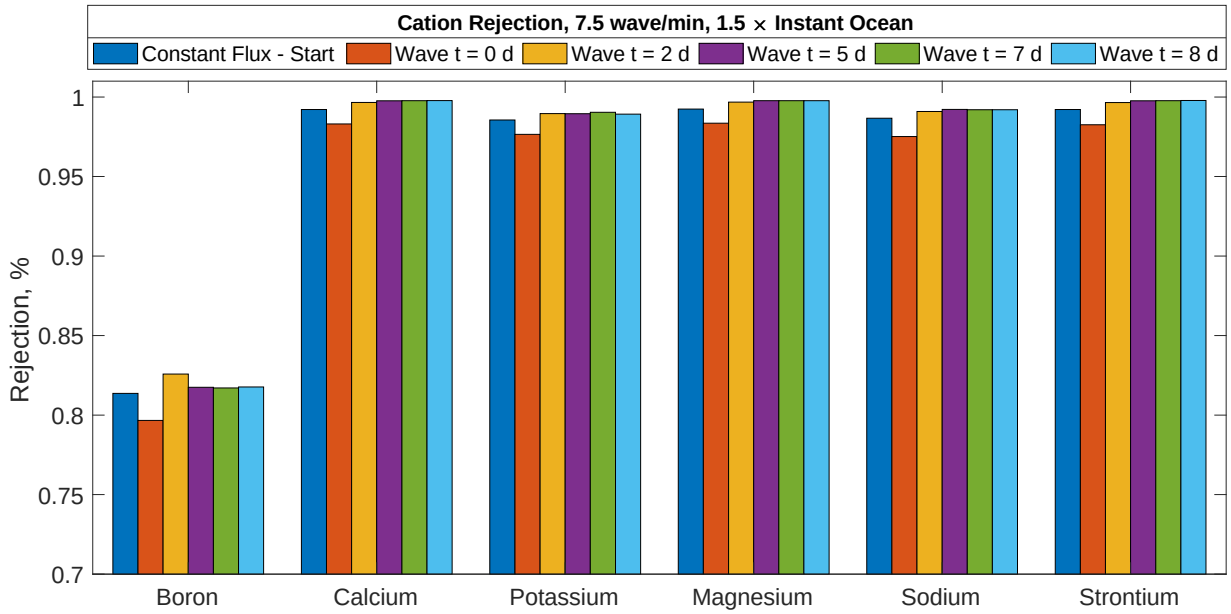

Fig. 9. Rejection efficiencies for B, Ca, K, Mg, Na, and Sr for experiments conducted with 1.5× Instant Ocean.

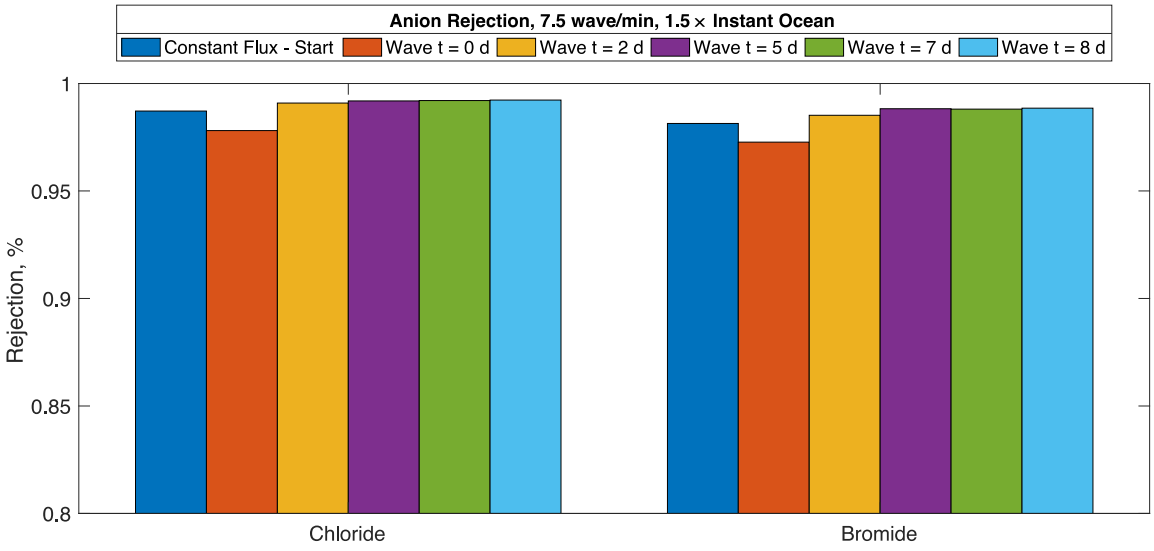

Fig. 10. Rejection efficiencies for Cl and Br for experiments conducted with 1.5× Instant Ocean.

For each of these experiments, the feed pressure was variable, resulting in variable flux over the spectrum of feed pressures. The concentrations of major cations over the spectrum of fluxes in each of the experiments are shown in Fig. 11, and the concentrations of Cl and Br are shown in Fig. 12. The gray line on each plot represents the average concentration for each element for all

experiments with Instant Ocean. These results show that at lower fluxes, the concentration of some of these elements may produce water that is either unsafe or unpalatable. For example, the average boron concentration in three experiments was 0.58 mg/L, which is slightly above the WHO guideline of 0.50 mg/L, for flux of approximately 14–35 LMH. These samples were composite samples, so were intended to reflect what the concentration might be for the end user after going into water storage and/or to the distribution system. However, these were very controlled experiments that virtually guaranteed those conditions; in a deployed system, the permeate quality will be entirely dependent on the sea state. Thus, if the system is producing water with acceptable boron content at typical conditions of 14–35 LMH, the quality of water may decline for a less energetic sea condition that produced flux of, for example, 10–25 LMH. The same can be said for other ions and the impact on palatability. In a taste test, panelists found water with > 800 mg/L TDS to be the least palatable, and it was particularly influenced by high concentrations of Na, K, and Cl [45]. Perhaps the biggest risk in operating a system that runs on variable feed pressure is not the impact to the membrane but planning for variable sea conditions. If the system is in a location where low flux and feed pressure is a possibility, the system should be designed with that in mind and possibly with a method for ensuring a minimum flux condition.

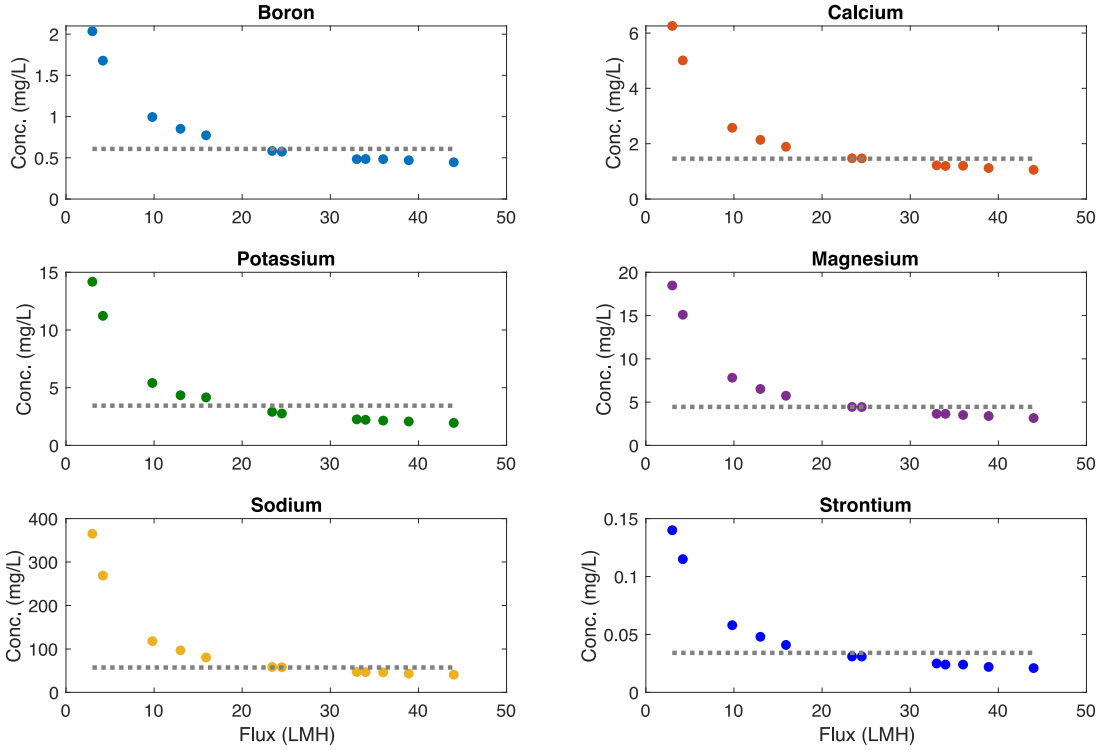

Fig. 11. The concentration of B, Ca, K, Mg, Na, and Sr in permeate water spanning the fluxes seen in each experiment. The gray lines represent the average permeate concentration in all experiments with Instant Ocean.

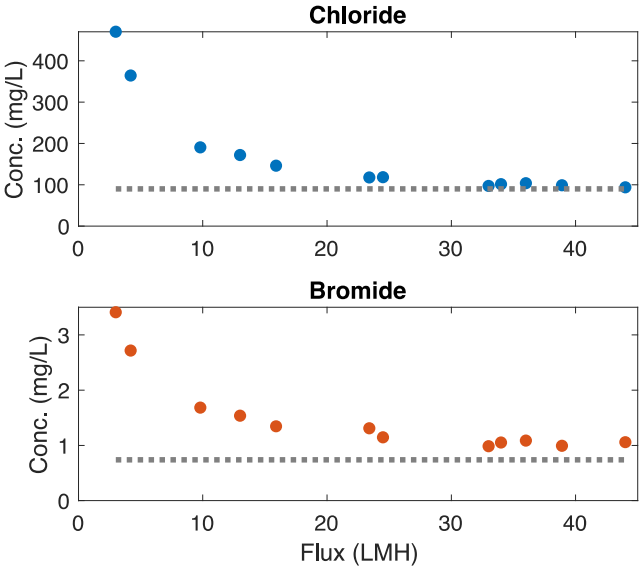

Fig. 12. The concentration of Cl and Br in permeate water spanning the fluxes seen in each experiment. The gray lines represent the average permeate concentration in all experiments with Instant Ocean.

4. Conclusion

This research presents the results of RO experiments conducted with feed pressure swings up to 400 psi (2.75 MPa) using feed compositions of NaCl and synthetic seawater. The experiments provide a baseline understanding of the impacts of consistent large pressure swings on membrane integrity and permeate quality that are needed for further development of WDDS. Membrane integrity was not shown to be impacted significantly by variable feed pressure experiments, as evidenced by the minimal changes in critical performance parameters such as the water permeability coefficient that was calculated during constant flux periods and between each experiment. In addition, though permeate conductivity varied as expected with increasing and decreasing feed pressure, cation and anion rejections and concentrations in product water fell within expected and acceptable ranges. Wave conditions also impacted permeate quality, with longer waves yielding lower salinity permeate, suggesting that a WDDS could benefit from the inclusion of technology capable of smoothing the power output from smaller wave periods if they are present. These results present no indication that further development in membrane technology

is needed to continue research in this area. This is a welcome result of experiments for which more membrane deterioration could be hypothesized; the membrane behaved as might be expected if the experiments were run under typical constant feed conditions. Experimentation built on this work should include multi-element configurations, longer term trials with different membrane modules, and further experimentation with more realistic waveforms than simple sine waves.

A WDDS has many potential applications and can be part of the broader technological leap needed to bring safe drinking water to more people while reducing greenhouse gas emissions. It also has other potential applications, including for quick deployment to coastal areas impacted by natural disasters and military installations. Because energy consumption accounts for the bulk of desalination operating costs, systems coupled with a large sustainable energy resource could reduce the specific energy consumption and, therefore, the unit cost of water delivered. Further, using wave energy directly to pressure feed water eliminates the need for some components typically found in current systems, such as a turbine, electrical generator, electric motor, and hydraulic pump, likely resulting in more efficient energy use. There are also potential cost savings associated with brine disposal for a WDDS because the system would be located in, or in very close proximity to, its brine disposal point (the ocean). Thus, the possible energy and cost savings from a fully realized WDDS warrant continued research and development, and the results from this work invite many more research questions.

Research toward the development of wave-driven RO systems is still in the beginning stages. This research represents the first step toward not only fabricating and deploying a WDDS, but also understanding the membrane processes and phenomena in play. However, more fundamental research should be conducted before engaging in system design. Much of what is understood about membrane processes assumes a constant feed condition, but when that condition changes, established concepts need to be reevaluated. Research is needed on the fouling and scaling tendencies of a membrane subject to wide pressure variations because fouling and scaling are significant considerations for engineering membrane treatment systems and can impact feed pressure itself. Similarly, concentration polarization results from constant feed pressure and flow should be better understood when operating under variable feed conditions. Further understanding and experimentation of larger design concepts, like membrane element configuration and process flow, will help build on the results presented here. Efforts to understand these phenomena under potential WDDS conditions will aid in system design, membrane technology development, and

modeling efforts. Aside from technology fundamentals, deploying a WDDS presents a new paradigm for membrane technology scientists and engineers. Like any other RO system, feed water in a WDDS needs to undergo some type of pretreatment. This presents unique challenges for a system that could exist entirely underwater and for a pretreatment technology that would be subject to variable feed conditions itself. There are similar challenges presented for system maintenance, product water distribution and delivery, and other aspects of water treatment engineering beyond pretreatment.

Acknowledgements

This work was authored in part by the National Renewable Energy Laboratory, operated by Alliance for Sustainable Energy, LLC, for the U.S. Department of Energy (DOE) under Contract No. DE-AC36-08GO28308. Funding provided by the U.S. Department of Energy Office of Energy Efficiency and Renewable Energy Water Power Technologies Office. The views expressed in the article do not necessarily represent the views of the DOE or the U.S. Government. The U.S. Government retains and the publisher, by accepting the article for publication, acknowledges that the U.S. Government retains a nonexclusive, paid-up, irrevocable, worldwide license to publish or reproduce the published form of this work, or allow others to do so, for U.S. Government purposes. Additionally, the authors would like to thank Michael Veres for his design and fabrication of the system used to conduct these experiments and for his continued assistance with troubleshooting and system maintenance.

References

[1] Z. Li, A. Siddiqi, L.D. Anadon, V. Narayanamurti, Towards sustainability in water-energy nexus: Ocean energy for seawater desalination, *Renewable and Sustainable Energy Reviews*, 82 (2018) 3833-3847. doi: 10.1016/j.rser.2017.10.087.

[2] M.A. Abdelkareem, M. El Haj Assad, E.T. Sayed, B. Soudan, Recent progress in the use of renewable energy sources to power water desalination plants, *Desalination*, 435 (2018) 97-113. doi: 10.1016/j.desal.2017.11.018.

[3] Q. Ma, H. Lu, Wind energy technologies integrated with desalination systems: Review and state-of-the-art, *Desalination*, 277 (2011) 274-280. doi: 10.1016/j.desal.2011.04.041.

[4] M.S. Miranda, D. Infield, A wind-powered seawater reverse-osmosis system without batteries, *Desalination*, 153 (2003) 9-16. doi: 10.1016/s0011-9164(02)01088-3.

[5] V.J. Subiela, J.A. Carta, J. González, The SDAWES project: lessons learnt from an innovative project, *Desalination*, 168 (2004) 39-47. doi: 10.1016/j.desal.2004.06.167.

[6] M. Freire-Gormaly, A.M. Bilton, Experimental quantification of the effect of intermittent operation on membrane performance of solar powered reverse osmosis desalination systems, *Desalination*, 435 (2018) 188-197. doi: 10.1016/j.desal.2017.09.013.

[7] R. Valladares Linares, Z. Li, S. Sarp, S.S. Bucs, G. Amy, J.S. Vrouwenvelder, Forward osmosis niches in seawater desalination and wastewater reuse, *Water research*, 66 (2014) 122-139. doi: 10.1016/j.watres.2014.08.021.

[8] M. Folley, B. Peñate Suarez, T. Whittaker, An autonomous wave-powered desalination system, *Desalination*, 220 (2008) 412-421. doi: 10.1016/j.desal.2007.01.044.

[9] N. Sharmila, P. Jalihal, A. Swamy, M. Ravindran, Wave powered desalination system, *Energy*, 29 (2004) 1659-1672. doi: 10.1016/j.energy.2004.03.099.

[10] J. Leijon, C. Boström, Freshwater production from the motion of ocean waves – A review, *Desalination*, 435 (2018) 161-171. doi: 10.1016/j.desal.2017.10.049.

[11] J. Leijon, J. Forslund, K. Thomas, C. Boström, Marine Current Energy Converters to Power a Reverse Osmosis Desalination Plant, *Energies*, 11 (2018) 2880. doi: 10.3390/en11112880.

[12] A. LiVecchi, A. Copping, D. Jenne, A. Gorton, R. Preus, G. Gill, R. Robichaud, R. Green, S. Geerlofs, S. Gore, D. Hume, W. McShane, C. Schmaus, H. Spence, US Department of Energy, Powering the Blue Economy: Exploring Opportunities for Marine Renewable Energy in Maritime Markets, 2019.

[13] US Department of Energy, Marine and Hydrokinetic Distributed and Alternate Applications Backgrounder, 2017.

[14] M. Qasim, M. Badrelzaman, N.N. Darwish, N.A. Darwish, N. Hilal, Reverse osmosis desalination: A state-of-the-art review, *Desalination*, 459 (2019) 59-104. doi: 10.1016/j.desal.2019.02.008.

[15] K. Wang, A.A. Abdalla, M.A. Khaleel, N. Hilal, M.K. Khraisheh, Mechanical properties of water desalination and wastewater treatment membranes, *Desalination*, 401 (2017) 190-205. doi: 10.1016/j.desal.2016.06.032.

[16] S. Jiang, Y. Li, B.P. Ladewig, A review of reverse osmosis membrane fouling and control strategies, *The Science of the total environment*, 595 (2017) 567-583. doi: 10.1016/j.scitotenv.2017.03.235.

[17] Y.-H. Yu, D.S. Jenne, Analysis of a Wave-Powered, Reverse-Osmosis System and Its Economic Availability in the United States, *American Society of Mechanical Engineers' International Conference on Ocean, Offshore and Arctic Engineering*, Trondheim, Norway, 2017.

[18] A.M. Cornett, A Global Wave Energy Resource Assessment, *The Eighteenth International Offshore and Polar Engineering Conference*, Vancouver, Canada, 2008.

[19] A. Sagiv, N. Avraham, C.G. Dosoretz, R. Semiat, Osmotic backwash mechanism of reverse osmosis membranes, *Journal of Membrane Science*, 322 (2008) 225-233. doi: 10.1016/j.memsci.2008.05.055.

[20] M. Al-haj Ali, A. Ajbar, E. Ali, K. Alhumaizi, Optimization-based periodic forcing of RO desalination process for improved performance, *Desalination and Water Treatment*, 51 (2013) 6961-6969. doi: 10.1080/19443994.2013.791767.

[21] A. Emad, A. Ajbar, I. Almutaz, Periodic control of a reverse osmosis desalination process, *Journal of Process Control*, 22 (2012) 218-227. doi: 10.1016/j.jprocont.2011.09.001.

[22] A.A. Abufayed, Performance characteristics of a cyclically operated seawater desalination plant in Tajoura, Libya, *Desalination*, 156 (2003) 59-65. doi: 10.1016/s0011-9164(03)00325-4.

[23] N.M. Al-Bastaki, A. Abbas, Periodic Operation of a Reverse Osmosis Water Desalination Unit, *Separation Science and Technology*, 33 (1998) 2531-2540. doi: 10.1080/01496399808545317.

[24] N.M. Al-Bastaki, A. Abbas, Improving the permeate flux by unsteady operation of a RO desalination unit, *Desalination*, 123 (1999) 173-176. doi: 10.1016/s0011-9164(99)00072-7.

[25] T.J. Kennedy, R.L. Merson, B.J. McCoy, Improving permeation flux by pulsed reverse osmosis, *Chemical Engineering Science*, 29 (1974) 1927-1931. doi: 10.1016/0009-2509(74)85010-4.

[26] A. Abbas, N. Al-Bastaki, Flux enhancement of RO desalination processes, *Desalination*, 132 (2000) 21-27. doi: 10.1016/s0011-9164(00)00131-4.

[27] M.A.-h. Ali, A. Ajbar, E. Ali, K. Alhumaizi, Study of cyclic operation of RO desalination process, *The Canadian Journal of Chemical Engineering*, 89 (2011) 299-303. doi: 10.1002/cjce.20407.

[28] Y.-H. Yu, D. Jenne, Numerical Modeling and Dynamic Analysis of a Wave-Powered Reverse-Osmosis System, *Journal of Marine Science and Engineering*, 6 (2018) 132. doi: 10.3390/jmse6040132.

[29] T.Y. Cath, M. Elimelech, J.R. McCutcheon, R.L. McGinnis, A. Achilli, D. Anastasio, A.R. Brady, A.E. Childress, I.V. Farr, N.T. Hancock, J. Lampi, L.D. Nghiem, M. Xie, N.Y. Yip, Standard Methodology for Evaluating Membrane Performance in Osmotically Driven Membrane Processes, *Desalination*, 312 (2013) 31-38. doi: 10.1016/j.desal.2012.07.005.

[30] A. Toffoli, E.M. Bitner-Gregersen, Types of Ocean Surface Waves, Wave Classification, (2017) 1-8. doi: 10.1002/9781118476406.emoe077.

[31] S.M. Riley, D.C. Ahoor, T.Y. Cath, Enhanced biofiltration of O&G produced water comparing granular activated carbon and nutrients, *The Science of the total environment*, 640-641 (2018) 419-428. doi: 10.1016/j.scitotenv.2018.05.228.

[32] L.F. Greenlee, D.F. Lawler, B.D. Freeman, B. Marrot, P. Moulin, Reverse osmosis desalination: water sources, technology, and today's challenges, *Water research*, 43 (2009) 2317-2348. doi: 10.1016/j.watres.2009.03.010.

[33] J. Kim, K. Park, D.R. Yang, S. Hong, A comprehensive review of energy consumption of seawater reverse osmosis desalination plants, *Applied Energy*, 254 (2019) 113652. doi: 10.1016/j.apenergy.2019.113652.

[34] P.A. Davies, Wave-powered desalination: resource assessment and review of technology, *Desalination*, 186 (2005) 97-109. doi: 10.1016/j.desal.2005.03.093.

[35] S. Kim, Osmotic pressure-driven backwash in a pilot-scale reverse osmosis plant, *Desalination and Water Treatment*, 52 (2013) 580-588. doi: 10.1080/19443994.2013.826771.

[36] A. Sagiv, R. Semiat, Backwash of RO spiral wound membranes, *Desalination*, 179 (2005) 1-9. doi: 10.1016/j.desal.2004.11.050.

[37] A. Panagopoulos, K.J. Haralambous, M. Loizidou, Desalination brine disposal methods and treatment technologies - A review, *The Science of the total environment*, 693 (2019) 133545. doi: 10.1016/j.scitotenv.2019.07.351.

[38] N. Prihasto, Q.-F. Liu, S.-H. Kim, Pre-treatment strategies for seawater desalination by reverse osmosis system, *Desalination*, 249 (2009) 308-316. doi: 10.1016/j.desal.2008.09.010.

[39] T. Mohammadi, M. Kazemimoghadam, M. Saadabadi, Modeling of membrane fouling and flux decline in reverse osmosis during separation of oil in water emulsions, *Desalination*, 157 (2003) 369-375. doi: 10.1016/s0011-9164(03)00419-3.

[40] R.A. Maltos, J. Regnery, N. Almaraz, S. Fox, M. Schutter, T.J. Cath, M. Veres, B.D. Coday, T.Y. Cath, Produced water impact on membrane integrity during extended pilot testing of forward osmosis – reverse osmosis treatment, *Desalination*, 440 (2018) 99-110. doi: 10.1016/j.desal.2018.02.029.

[41] W. Guo, H.H. Ngo, J. Li, A mini-review on membrane fouling, *Bioresource technology*, 122 (2012) 27-34. doi: 10.1016/j.biortech.2012.04.089.

[42] P. Ramakul, N. Leepipatpiboon, C. Yamoum, U. Thubsuang, S. Bunnak, U. Pancharoen, Reduction of concentration polarization at feeding interphase of a hollow fiber supported liquid membrane by using periodic operation, *Korean Journal of Chemical Engineering*, 26 (2009) 765-769. doi: 10.1007/s11814-009-0128-4.

[43] G. Patroklou, K.M. Sassi, I.M. Mujtaba, Simulation of boron rejection by seawater reverse osmosis desalination, *The 11th International Conference on Chemical and Process Engineering*, Milan, Italy, 2013.

[44] D. Prats, M.F. Chillon-Arias, M. Rodriguez-Pastor, Analysis of the influence of pH and pressure on the elimination of boron in reverse osmosis, *Desalination*, 128 (2000) 269-273. doi: 10.1016/s0011-9164(00)00041-2.

[45] S. Platikanov, V. Garcia, I. Fonseca, E. Rullan, R. Devesa, R. Tauler, Influence of minerals on the taste of bottled and tap water: a chemometric approach, *Water research*, 47 (2013) 693-704. doi: 10.1016/j.watres.2012.10.040.